The nature of disorder in montmorillonite by simulation of X-ray powder patterns

ALBERTO VIANI,[1] ALESSANDRO F. GUALTIERI,[2,*] AND GILBERTO ARTIOLI[3]

[1]Eurosabbie Eurominerali, Poviglio, Reggio I-42028, Italy
[2]Dipartimento di Scienze della Terra, Università di Modena e Reggio Emilia, I-41100 Modena, Italy
[3]Dipartimento di Scienze della Terra, Università di Milano I-20133 Milano, Italy

ABSTRACT

The planar disorder of Ca-montmorillonite (Fuller's earth) has been investigated using structural simulations of X-ray powder patterns. A standard sample was fully characterized using chemical, microscopic, and diffraction methods. Earlier models of disorder taken from the literature and newly formulated combined models were used to generate simulated powder patterns to be compared with the experimental spectrum.

A new model of disorder with random shifts of $-\mathbf{a}/3$ and $\pm\mathbf{b}/3$, with a total density of defects of 75%, gives the best fit to the observed data. Thus, the sample cannot be classified as a turbostratic structure (fully disordered) and consequently turbostratic disorder does not invariably apply to all smectite samples. These findings open a debate on the nature and application of turbostratic disorder: is it possible for smectite samples to have intermediate degrees of disorder between a fully disordered stacking (turbostratic) and a highly faulted but well-defined stacking or is the result obtained for the Ca-montmorillonite just an exception?

This model of disorder is useful for the quantitative phase analysis by X-ray powder diffraction based on the Rietveld method, which can now benefit from a more reliable initial structure model for Ca-montmorillonite and which will improve the accuracy of the weight-fraction estimates.

INTRODUCTION

Smectite minerals are constituents of soils and are the main component of *bentonite* rocks. The structural formula of dioctahedral aluminous smectites in the series montmorillonite-beidellite is $(Al_{2-y}Mg_y)(Si_{4-x}Al_x)O_{10}(OH)_2E_{x+y}\cdot nH_2O$ when $y > x$, smectite is called *montmorillonite* (Güven 1988). The basic silicate building block is composed of a 2:1 structure with an octahedral layer sandwiched between two tetrahedral layers. If we describe the structure in its ideal monoclinic symmetry, there are, in principle, three octahedral cavities per unit cell. The cavity on the mirror plane designated M1 is usually vacant in the dioctahedral species, and the other two cavities to the left and right of the mirror plane are designated M2. M1 sites have a trans configuration (i.e., hydroxyls are across the site), whereas M2 sites display a cis configuration (i.e., hydroxyls are adjacent on one side of the coordination polyhedron). A configuration with vacant trans sites M1 produces an elementary layer with $C2/m$ symmetry when the cis sites are occupied by the same element (Zvyagin and Pinsker 1949). Another arrangement where the trans M1 site and one of the cis sites are occupied gives $C2$ symmetry (Méring and Oberlin 1971; Tsipursky and Drits 1984).

Several substitutions may take place in either octahedral and/or tetrahedral sites, whose net charge compensation requires the presence of cations and water molecules in the interlayer region. Univalent and divalent cations are the most common substitutes in the interlayer space. The known interlayer sites favorable for a cation without a hydration shell are located at the center of the O atom triad corresponding in projection with the tetrahedral cation and within the hexagonal cavities closer to two basal and one apical O atom of the tetrahedra with R^{3+} substitutions. The most favorable position for the divalent compensating cations is at the center of two adjacent basal O atom triads belonging to adjacent layers, thus forming sixfold coordination in various geometries. Divalent cations can also occur in the hexagonal cavities coordinating two charged O atoms from each adjacent layer. The hexagonal cavity is the most favorable position for monovalent cations (12-fold coordination).

A basic feature of montmorillonite (and smectites in general) is the stacking of elementary layers with the diffraction patterns showing only two types of reflections: the basal (00*l*) and the unmodulated (*hk*0) bands corresponding to a two-dimensional diffraction (Drits et al. 1984). Méring (1975) described three stacking modes: (1) *regular*, with zero degree rotations between successive layers in a pseudohexagonal arrangement with a perfect 3D periodicity. This mode is rarely observed for dioctahedral smectites, (2) *semi-random*, with $n \times 60°$ rotations. Hexagonal cavities are retained and only the (*hkl*) reflections with $k = 3n$ are observed, (3) *turbostratic*, with completely random rotations and translations between adjacent

* E-mail: alex@unimo.it

layers with no hexagonal coordination cavities (extensive planar disorder), that is, the layers are displaced from each other in the **a-b** plane by random amounts and are rotated about the normal by random amounts (Moore and Reynolds 1989). Only the (00l) (optically coherent) and broad (hk0) bands are visible. This is the common mode for dioctahedral smectites and almost all smectite minerals where the weakly bonded exchangeable cations force no ordering.

Layer stacking is generally influenced by the nature of the interlayer cation, the nature and number of solvation molecules, the di- or trioctahedral character of the mineral, the mean crystallite size, and the ordering of interlayer cations over the available hexagonal cavities.

Unfortunately, although planar disorder is a distinctive character of montmorillonite that strongly influences the physical properties, there are no conclusive models in the literature so far. The attempts of Tsipursky and Drits (1984) to model disorder of montmorillonite in terms of octahedral site vacancies and Drits et al. (1984) to model disorder of K-saturated montmorillonite are only partial and several different models may be optionally considered.

Obviously, a quantitative or even a semi-quantitative model of the nature of disorder in montmorillonite would help with understanding phenomena such as dehydration/dehydroxylation reactions (Bray and Redfern 1999), as well as physical properties and use. Besides, the quantitative phase analysis (QPA) by X-ray powder diffraction based on full profile fitting or the Rietveld method, would take advantage of a reliable structure model of disorder for montmorillonite, because the estimate of the weight fraction is strongly dependent on the assumed structure models (Gualtieri 1999b).

The reasons above prompted this study on the nature of disorder in Ca-montmorillonite through analysis of a representative sample from Texas. Earlier models taken from the literature and a new one of disorder of Ca-montmorillonite were used to calculate powder patterns to be compared to the observed spectrum. This strategy was successfully used in the past for the description of disorder in kaolinite (Artioli et al. 1995) and talc (Gualtieri 1999a). To do this, we made use of the program DIFFaX (Treacy et al. 1991), which was specifically developed to study extensively faulted crystals. Extensive planar disorder that causes broadening of the Bragg peaks in the diffraction pattern can be described using a mathematical model (Hendricks and Teller 1942; Wilson 1943; Allegra 1964; Warren 1959; Cowley 1976; Brindley 1980). Treacy et al. (1991) used a recursion algorithm (Michalski 1988; Michalski et al. 1988) to simulate diffraction effects in one-dimensional disorder. The program DIFFaX was written to take full advantage of the flexibility of such a general algorithm. Recursion gives a set of simple relations between average interference terms from a statistical crystal that can be solved as a set of simultaneous equations. The details of the algorithm and the theoretical aspects are fully described in Treacy et al. (1991). The program produces simulated powder patterns to be compared with observed ones, thus providing some verification of the reliability of a structure model. Besides simulation of powder patterns, the investigation of the structure disorder of kaolinite was performed with the aid of ab initio lattice energy calcula-

tions. In the literature, different methods are described for the calculation of lattice energy: quantum-mechanics using the ab initio Hartree-Fock method (Hess and Saunders 1992); semiempirical methods (Collins and Catlow 1991; Bleam 1993; Artioli et al. 1995), molecular dynamics simulations (Chang et al. 1997), quantum chemical calculations using both semiempirical and first principle potentials (Chatterjee et al. 1997); molecular simulations using empirical force field potentials (Čapková et al. 1998), and Monte Carlo simulations (Sposito et al. 1998). Such calculations are precluded here for several reasons. The positions of the protons of the water molecules are unknown and thus cannot be included in the ab initio model. The population of the interlayer cation and water molecules is partial, that is, in order to correctly account for the site population, an enormous $n \times n$ supercell should be considered, making the ab initio calculation too time consuming to be performed. Even with the approximation of full site occupancy, some models of disorder imply the use of supercells with more than 200 atoms again preventing the ab initio approach.

EXPERIMENTAL METHODS

Sample selection

A survey of the literature data that reports X-ray powder patterns of montmorillonite samples revealed that they are mainly classified into Ca-rich, Na-rich, and Ni-rich varieties. Table 1 reports the peak positions and relative intensity of the five most representative samples described in the literature. Differences in the nature of the interlayer compensating cation (Ca^{2+}, Na^+, or Ni^{2+}) strongly influences the position of the first peak and the relative intensity and position of the other minor peaks/bands. All the samples show a weak-medium peak at 5.0–5.2 Å, a medium-strong asymmetric band at 4.5 Å, and weak broad bands in the regions around 2.5–2.6 Å and 1.5–1.7 Å. Several minor peaks are shown by the Ca-rich samples.

In this study, we selected the Ca-rich sample from Texas to study the nature of disorder in montmorillonite. The Ca-rich sample was selected instead of the Na-rich material primarily because Ca is a stronger X-ray scatterer, and its contribution to the modification of the structure factors (peak intensities) in the powder patterns can be better evidenced and evaluated. In fact, the scattering power of Na is comparable to that of the water molecules and thus is hard to discriminate. On the other hand, the Ni-sample was not considered as representative of the natural samples as it was the result of cation exchange of a Fe-rich sample in nickel chloride solution (Muller et al. 1997).

Sample characterization

The chemical analysis (wt% oxides) of the sample taken from the literature (van Olphen and Fripiat 1978) is: SiO_2 = 70.1, Al_2O_3 = 16.0, TiO_2 = 0.22, Fe_2O_3 = 0.65, FeO = 0.15, MnO = 0.009, MgO = 3.69, CaO = 1.59, Na_2O = 0.27, K_2O = 0.078, P_2O_5 = 0.026, CO_2 = 0.16. H_2O determined by TG analysis is 6.54 wt%. It is not possible to calculate a reliable structure formula because a small amount of cristobalite (<5 wt%) was found in the sample. SEM images (available upon request to the authors) showed that the average grain size of the pow-

TABLE 1. The peak positions and relative intensities of the five most representative montmorillonite samples described in the literature

Ca-montmorillonite STx-1 Texas (this study)		Ca-montorillonite (Bayliss 1989)		Na-montmorillonite SWy-1 Wyoming (Van Olphen and Fripiat 1978)		Ca,Na-montorillonite (Molloy and Kerr 1961)		Ni-montmorillonite (Muller et al. 1997)	
				Peak position (Å) and relative intensity					
2θ	I	2θ	I	2θ	I	2θ	I	2θ	I
16	100	15.0	100	–	–	–	–	16.7	100
–	–	–	–	13.6	100	13.6	100	–	–
–	–	–	–	–	–	–	–	8.3	4
5.1	4	5.0	60	5.2	12	–	–	5.6	6
4.5	16	4.5	80	4.5	65	4.5	18	4.4	18
4.1*	12	–	–	–	–	–	–	–	
–	–	3.8	20	–	–	–	–	–	–
–	–	3.5	10	–	–	–	–	–	–
–	–	3.3	10	–	–	3.3	10	3.3	10
3.1	4	–	–	–	–	3.2	10	3.1	1
–	–	3.0	60	–	–	2.9	8	–	–
2.6	3	2.6	40	2.6	18	2.6	5	–	–
2.5	3	2.5	40	–	–	2.5	5	2.5	9
–	–	2.3	10	–	–	–	–	–	–
2.0†	2	2.1	10	–	–	–	–	–	–
–	–	1.9	10	–	–	–	–	–	–
1.7	1	1.7	30	1.7	8	–	–	1.7	4
–	–	1.5	50	1.5	12	–	–	1.5	9
–	–	1.3	20	–	–	–	–	–	–
–	–	1.2	20	–	–	–	–	–	–

* Cristobalite.
† Al (holder).

der sample is less than 1 mm. TEM images (available upon request to the authors) showed that the average particle size of montmorillonite is nanometric in agreement with the surface area, which is 83.7(2) m²/g (van Olphen and Fripiat 1978) and yields a mean crystal thickness of 9.5 nm according to the relationship T = 800/S (Nadeau 1985) with T, the sample thickness in nm and S, the surface area in m²/g. Cristobalite crystals present as impurities display a much larger size.

Prior to the laboratory analyses, the sample was hand ground in an agate mortar for about 10 min without the use of a liquid phase. A maximum diameter of the particle aggregates of about 1–2 mm was confirmed by laser diffraction which showed a Gaussian peak of size distribution centered at about 1.2 mm. The powder was then side loaded in a flat aluminum holder for X-ray data collection on a Philips conventional Bragg-Brentano vertical diffractometer with CuKα radiation and a pyrolitic graphite crystal monochromator mounted on the diffracted-beam. Data were recorded in the range 3–70 °2θ with steps of 0.02 °2θ and 20 s per step. The observed powder pattern is shown in Figure 1. Cristobalite present as an impurity (label C in Fig. 1) was modeled using GSAS (Larson and Von Dreele 1994) and subtracted from the original pattern.

Structure simulations of X-ray powder patterns

The model of Tsipursky and Drits (1984) with space group $C2/m$ (see Table 3 on p. 512 in Güven 1988: note that M2 ≡ M3, T1 ≡ T2, O2 ≡ O3, and O5 ≡ O6) was used to prepare the starting calculated model for the structural simulations in DIFFaX (Treacy et al. 1991). With respect to the 10 Å dehydrated model of Tsipursky and Drits (1984), Ca was substituted for K and the z atomic coordinates rescaled to create a 15 Å unit. This model was then transformed into a more flexible and versatile triclinic $P\bar{1}$ orthogonalized unit (all the angles = 90°) with $a = 5.18$ Å, $b = 8.98$ Å, and $c = 15.00$ Å in order to make it easier to use in DIFFaX. Table 2 reports the list of the

transformed atomic coordinates used as initial DIFFaX input. The stacking vector in DIFFaX (–0.5628 along a, 0.0 along b, and 1.0 along c) accounts for the monoclinic distortion to the orthogonalized system.

Every model of disorder is defined by a probability matrix of stacking of the layers; explanations and details can be found in Treacy et al. (1991) and Artioli et al. (1995). The various models were obtained in different ways, and the translational disorder was obtained by application of the shift vector ($\mathbf{a}/3$, $-\mathbf{a}/3$, $\mathbf{b}/3$, $-\mathbf{b}/3$) directly to the stacking vector. For example, a sequence with an ideal layer (1) and a $\mathbf{b}/3$ layer (2) is obtained with the following stacking transition vectors: from (1) to (1) with –0.5628 along a, 0.0 along b and 1.0 along c; from (1) to (2) with –0.5628 along a, 0.3333 along b and 1.0 along c; from (2) to (2) is equal to (1) to (1). The rotational disorder was
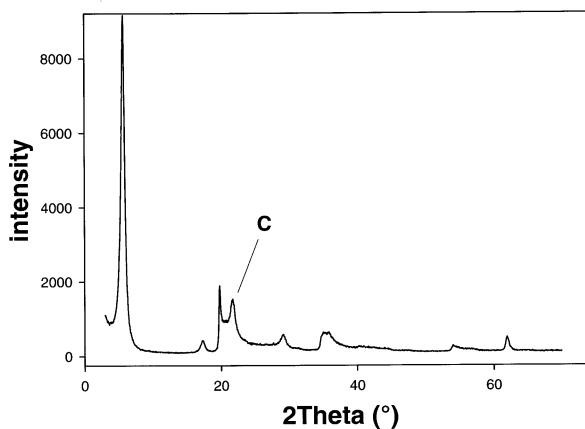

FIGURE 1. The observed powder pattern of Ca-montmorillonite. Cristobalite present as an impurity was modeled using GSAS and subtracted from the original pattern.

TABLE 2. Atomic coordinates, population and atomic displacement parameters of the idealized orthogonal *P*1 montmorillonite used in DIFFaX

Atom	x	y	z	U_{iso} (Å^2)	Population (%)
Al	0.8753	0.3330	0.2214	0.02	1.00
Al	0.8753	0.6670	0.2214	0.02	1.00
Al	0.3753	0.8330	0.2214	0.02	1.00
Al	0.3753	0.1670	0.2214	0.02	1.00
Si	0.5588	0.3290	0.0430	0.02	1.00
Si	0.5588	0.6710	0.0430	0.02	1.00
Si	0.6919	0.8290	0.3999	0.02	1.00
Si	0.6919	0.1710	0.3999	0.02	1.00
Si	0.0588	0.8290	0.0430	0.02	1.00
Si	0.0588	0.1710	0.0430	0.02	1.00
Si	0.1919	0.3290	0.3999	0.02	1.00
Si	0.1919	0.6710	0.3999	0.02	1.00
O	0.5134	0.5000	0.0099	0.02	1.00
O	0.8280	0.7280	0.0000	0.02	1.00
O	0.8280	0.2720	0.0000	0.02	1.00
O	0.4954	0.0000	0.1520	0.02	1.00
O	0.5682	0.6910	0.1487	0.02	1.00
O	0.5722	0.3090	0.1487	0.02	1.00
O	0.7373	0.0000	0.4329	0.02	1.00
O	0.4227	0.2280	0.4428	0.02	1.00
O	0.4227	0.7720	0.4428	0.02	1.00
O	0.7553	0.5000	0.2908	0.02	1.00
O	0.6824	0.1910	0.2941	0.02	1.00
O	0.6784	0.8090	0.2941	0.02	1.00
O	0.0134	0.0000	0.0099	0.02	1.00
O	0.3280	0.2280	0.0000	0.02	1.00
O	0.3280	0.7720	0.0000	0.02	1.00
O	0.9954	0.5000	0.1520	0.02	1.00
O	0.0682	0.1910	0.1487	0.02	1.00
O	0.0722	0.8090	0.1487	0.02	1.00
O	0.2373	0.5000	0.4329	0.02	1.00
O	0.9227	0.7280	0.4428	0.02	1.00
O	0.9227	0.2720	0.4428	0.02	1.00
O	0.2553	0.0000	0.2908	0.02	1.00
O	0.1824	0.6910	0.2941	0.02	1.00
O	0.1784	0.3090	0.2941	0.02	1.00
Ca	0.1893	0.0000	0.7215	0.02	0.50
Ca	0.6893	0.5000	0.7215	0.02	0.50

accomplished by application of the general rotation matrix [a_{11} = cosα; a_{12} = –sinα; a_{13} = 0; a_{21} = sinα; a_{22} = cosα; a_{23} = 0; a_{31} = 0; a_{32} = 0; a_{33} = 1 with α = 60, –60, 120, –120°] directly to the coordinates of the layer in order to obtain a rotated layer to be stacked with the same stacking vectors.

A pseudo-Voigt function was used to de-convolute the instrumental broadening h(2θ) using the coefficients calculated from the refinement of standard BaF$_2$ produced by Merck (suprapure quality) which was collected with the same experimental conditions as the investigated sample. The profile function of a powder pattern is assumed to be the convolution of the instrumental and microstructural broadening, according to the relation f(2θ) = g(2θ) * h(2θ), with g(2θ) = microstructural function, and h(2θ) = instrumental function (Young and Wiles 1982; Louër and Langford 1988; Langford et al. 1993; Van Berkum et al. 1996). Because BaF$_2$ annealed following the procedure described in Louër and Langford (1988) is considered to have no microstructural broadening, it can be successfully used to calculate the instrumental broadening h(2θ) of a given experimental setting. The coefficients of the pseudo-Voigt function were U = 1.0, V = –0.8, and W = 0.3 (Treacy et al. 1991) with mixing parameter η = 0.4.

The calculated patterns were compared to the observed data. The background was manually removed and the scale factor was varied to obtain the best fit. The final agreement was evalu-

ated using the factor R_p = {Σ |y_i(obs)–y_i(calc)| } /Σy_i(obs). A cross-check of the consistency of the calculated powder pattern of the idealized orthogonal structure was performed by calculating the pattern with GSAS and the results showed that the two patterns are in perfect agreement (Fig. 2: R_p = 0.011).

RESULTS

The first step was to investigate in a systematic way and categorize each factor, such as shifts, rotations, random substitutions or others, which may broaden diffraction lines in the powder pattern of montmorillonite. This strategy was inspired by the suggestion of Drits et al. (1984) who investigated the disorder of K-saturated montmorillonites: "*it would be instructive to adopt a more general approach to the problem of the real structure of smectites based on a systematic analysis of the relationship between structural characteristics and diffraction patterns*". The second step was to combine single factors to reproduce the actual model of disorder in montmorillonite.

The first factor to be considered is the position of Ca in the interlayer region. Ca can be found in the hexagonal cavities (simulation S1 in Fig. 3 and probability matrix S1 in Table 3) coordinating two O atoms from each adjacent layer or at the center of two adjacent O atom triads (simulation S2 in Fig. 3 and probability matrix S2 in Table 3) in a more or less distorted excess charge sixfold coordination. Ca at the center of the O atom triads requires Al in M1 (simulation S3 in Fig. 3 and probability matrix S3 in Table 3). Simulation S4 (Fig. 3 and probability matrix S4 in Table 3) is the combination of Ca at the center of the O atom triads and Al in M1. By comparison with the experimental pattern in Figure 1, it is clear that none of the simulations is capable of reproducing the relative peak intensities of the observed pattern and especially (002) and (003) in the 10–19 °2θ region and (113) and (005) in the 29–30 °2θ region which are markedly weaker (see also the large reported R_p values). The amount of Ca in the hexagonal cavity is also important when modeling the peak intensity. Figure 4 shows
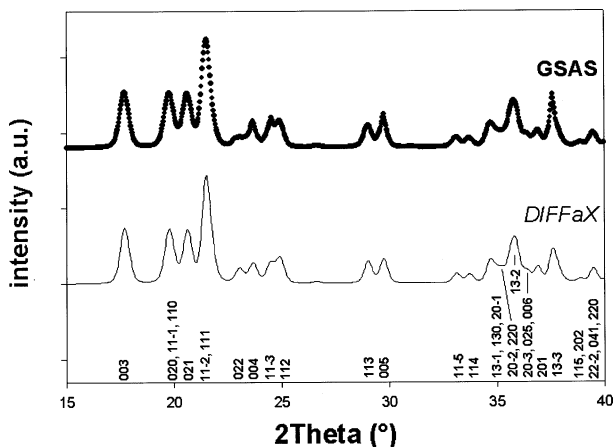

FIGURE 2. The calculated powder pattern in the range 15–40 °2θ for the ideal orthogonalized *P* 1 dehydrated 15 Å montmorillonite model used as input data for DIFFaX, the corresponding 15 Å dehydrated pattern calculated in the space group *C*2/*m* with GSAS, and relative Miller indices (see text for details).
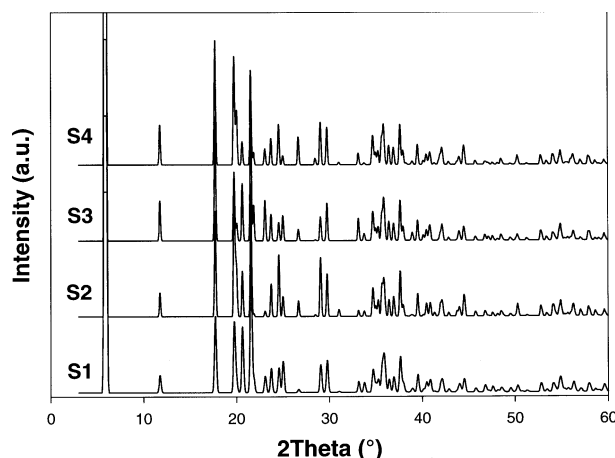
FIGURE 3. Set of DIFFaX structure simulations with Ca in different positions within the interlayer space.
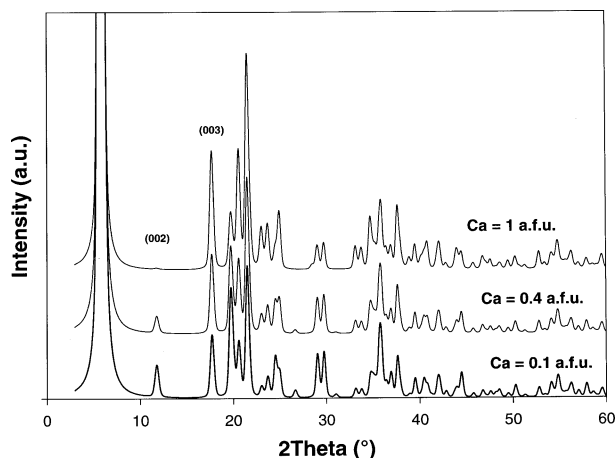

FIGURE 4. Set of DIFFaX structure simulations with increasing amount of Ca in the hexagonal cavity.

simulations with increasing amounts of Ca in the hexagonal cavity. For example, the reduction of the (003) reflection, as observed in the experimental pattern, seems to be related to the population of the Ca site.

Besides the ideal configurations in which the trans positions are vacant (the T layers in the description of Drits et al. 1984) and the cis positions are vacant (the C layers in the description of Drits et al. 1984), we tried to simulate the effect of a random occupancy of the octahedral sites in which Al statistically occupies both M1 and M2 sites (the M layers in the description of Drits et al. 1984). The result is shown in Figure 5. Simulation S5 was obtained by random distribution of Al over the octahedral sites (33% in M1 and 66% in the two equivalent M2 sites). Although simulation S5 refers to the M stacking model of Drits et al. (1984), it is important to stress that the simulated powder pattern is not directly comparable to the one reported on Figure 4, p. 549 of Drits et al. (1984) because, as

stated by the authors, they considered *only the models corresponding to dioctahedral smectites saturated by K-cations and collapsed* whereas the models here correspond to dioctahedral smectites saturated by Ca-cations and uncollapsed (15 Å unit with water molecules). In addition, further differences in the peak intensities may arise from differences in the thermal parameters, site populations, parameters of the peak profile function, and other factors intrinsic to the calculation method. In fact, this specific simulation was calculated in a recursive way on an infinite ensemble of random crystallites in DIFFaX whereas Drits et al. (1984) have chosen a mean number of layers $\bar{N} = 20$ and radius for the coherent domain in the **a**–**b** plane equal to 200 Å.

Simulation S6 was obtained by considering that when Al occupies M1, Ca in the interlayer region can be found just below the M1 octahedron. The simulations show that neither random distribution of Al in the octahedral cavities nor the

TABLE 3. The probability of layer existence* and R_p values of structure simulations S1–S17

Simulation	Ideal layer	Ca under the O atoms triad	Al in M1	Al in M1 and Ca under the oxygens triad	Al in M2	Water in W1	Water in W2	**b**/3 shift in W2	−**b**/3 shift	**a**/3 shifts	−**a**/3 shifts	R_p values†
S1	100	–	–	–	–	–	–	–	–	–	–	0.711
												0.011‡
S2	–	100	–	–	–	–	–	–	–	–	–	0.709
S3	–	–	100	–	–	–	–	–	–	–	–	0.707
S4	–	–	–	100	–	–	–	–	–	–	–	0.710
S5	–	–	50	–	50	–	–	–	–	–	–	0.700
S6	–	–	100	–	–	–	–	–	–	–	–	0.702
S7	–	–	–	–	–	100	–	–	–	–	–	0.711
S8	–	–	–	–	–	50	50	–	–	–	–	0.711
S9	20	–	–	–	–	–	–	40	40	–	–	0.495
S10	34	–	–	–	–	–	–	33	33	–	–	0.481
S11	50	–	–	–	–	–	–	25	25	–	–	0.487
S12	20	–	–	–	–	–	–	–	–	40	40	0.439
S13	34	–	–	–	–	–	–	–	–	33	33	0.444
S14	50	–	–	–	–	–	–	–	–	25	25	0.441
S15	25	–	–	–	–	–	–	25	25	–	25	0.412
S16	20	–	–	–	–	–	–	20	20	20	20	0.415
S17	4	–	–	–	–	–	–	24	24	24	24	0.444

* The probability of existence of the layers is calculated from the probability matrix of DIFFaX. For example, in a model with three layers with a 3×3 matrix corresponding to $a_{11} = 20$, $a_{12} = 40$, $a_{13} = 40$, $a_{21} = 40$, $a_{22} = 20$, $a_{23} = 40$, $a_{31} = 40$, $a_{32} = 40$, and $a_{33} = 20$, the probability of existence of each layer is 33%.
† By comparison with the observed file, defined as: $R_p = \{\Sigma |y_i(\text{obs}) - y_i(\text{calc})|\} / \Sigma y_i(\text{obs})$.
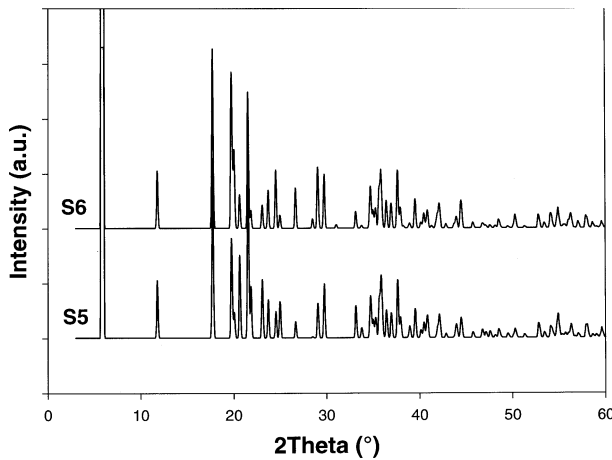‡ By comparison with the GSAS ideal structure.

FIGURE 5. Set of DIFFaX structure simulations with different octahedral layer configurations.

combined configuration with Al in M1 and Ca below the M1 octahedron yield remarkable modulations of the peaks. The intermediate 15–25 °2θ region in particular shows sharp and well defined diffraction peaks with inconsistently high relative intensities. Similar results not reported here were found by substituting Mg for Al in the ratio indicated by the chemical formula. The distortion effects around any vacant or occupied octahedral sites were not considered. This may be the reason for the inconsistency with the findings of Drits et al. (1984) that the distribution of the intensities for the (02*l*) and (11*l*) bands permits differentiation without ambiguity between T, C, and M stacking even in the presence of stacking faults.

Moreover, because we assumed that charge is concentrated in the octahedral sheet (a reasonable assumption for this sample) and given the nearly equal diffusion cross section of Si and Al for X-rays, random distribution of Al in place of Si in the tetrahedral sites was not considered.

The positions of the water molecules in the interlayer region which are coordinated to the Ca atoms were also investigated. Two positions labeled W1 and W2 (Figs. 6a and 6b) were taken into account. W1 has the same *x* and *y* coordinates of the Ca atoms and is displaced 0.19 along *z*. W2 is coplanar with the Ca atoms. When both are partially occupied, the coordination of Ca is eightfold. Simulation S7 was obtained with W1 alone whereas simulation S8 was obtained with both W1 and W2. The simulations (Fig. 6c) show that neither W1 alone nor a combined configuration with W1 and W2 result in significant modulation of the peaks. The intermediate 15–25 °2θ region shows sharp and well defined diffraction peaks with inconsistently high relative intensities (see also the large R_p values).

Shift disorder was investigated in the series of simulations whose calculated patterns are shown in Figure 7 (see the probability matrices in Table 3). Shifts may occur along the **b** axis with components of ±**b**/3 which retain the periodicity of the octahedral columns perpendicular to the **a**–**b** plane as these columns have a repetition step of **b**/3, or along the **a** axis with components ±**a**/3 as already observed for talc (Gualtieri 1999a)
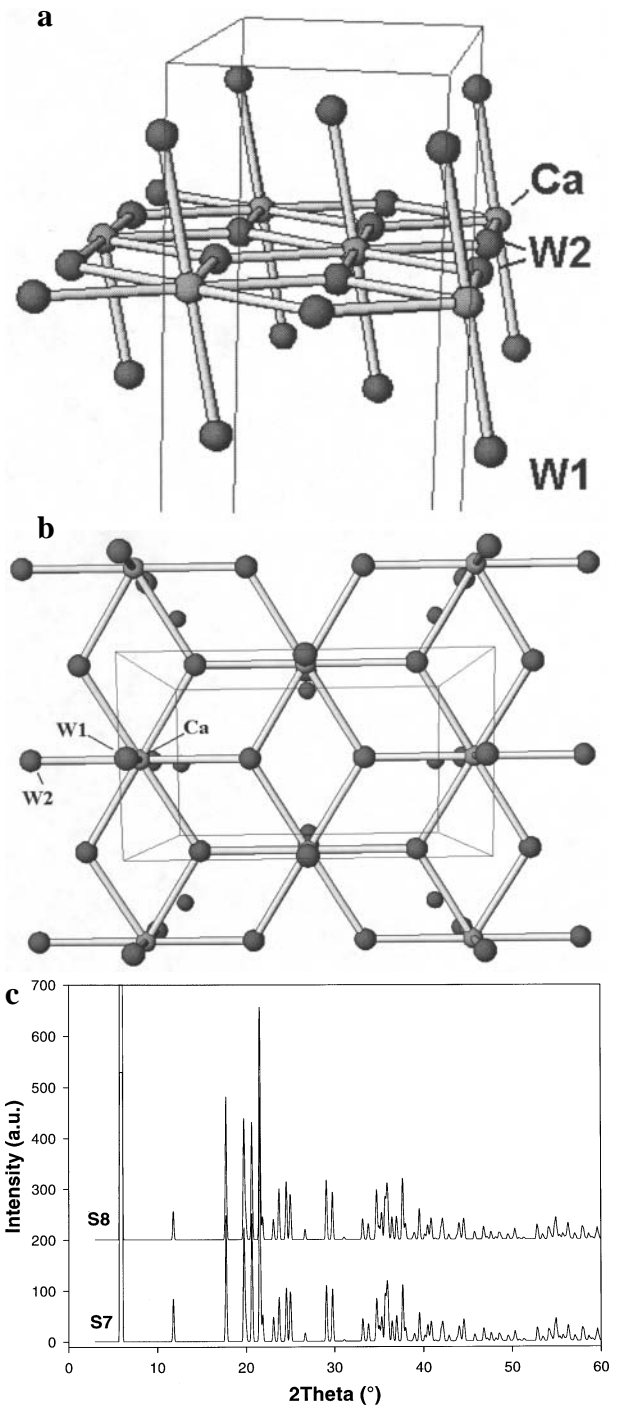

FIGURE 6. The different positions of the water molecules W1 (**a**) and W2 (**b**) in the interlayer region generating the set of DIFFaX structure simulations shown in (**c**).

which preserve the superposition of two out of three basal O atoms of two adjacent layers. The models with the **b**/3 shifts alone (simulations S9-S11) reproduce well the intermediate 15–25 °2θ region, but poorly reproduce the high angle (35–60 °2θ) region. In contrast, the models with ±**a**/3 shifts alone (simula-
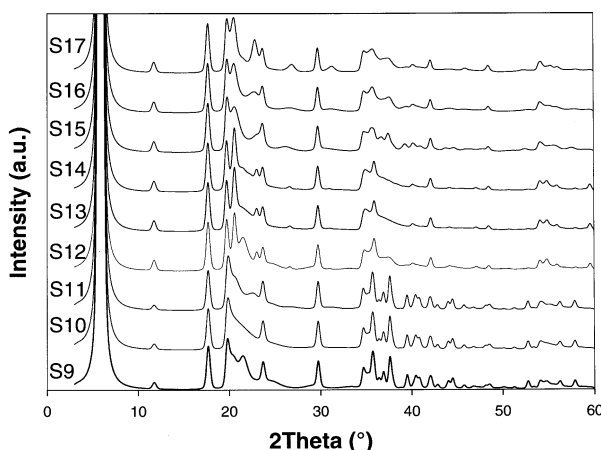
FIGURE 7. Set of DIFFaX structure simulations of models with translational disorder along ± **b**/3, ± **a**/3, and combined ± **b**/3 and ± **a**/3.

tions S12-S14) poorly reproduce the intermediate 15–25 °2θ region and correctly broaden the high angle (35–60 °2θ) region. The mixed models (simulations S15-S17) yield a satisfactory match with the full observed pattern (especially simulation S16) although some extra inconsistent peaks are still observed at 12.5, 24, and 42 °2θ.

Rotations between adjacent layers which preserve the superposition of basal O atoms of adjacent layers have been considered in the simulation series in Figure 8 (see the probability matrices in Table 4). Drits et al. (1984) have shown that mica-like stacking may lead to azimuthal defects corresponding to ±120° and ±60° rotations of successive layers and that the usual coordination of the compensating cation K is kept in the case of ±120° rotations while it becomes prismatic in the case of ±60° rotations. The simulations with 60° rotations only are S18-S19, and the simulations with only 120° rotations only are S20-S21. This simulation is in agreement with that reported in Figure 14(b) in Drits et al. (1984) for the same system showing the appearance of a sharp broad band at 22.3 °2θ. The simulations

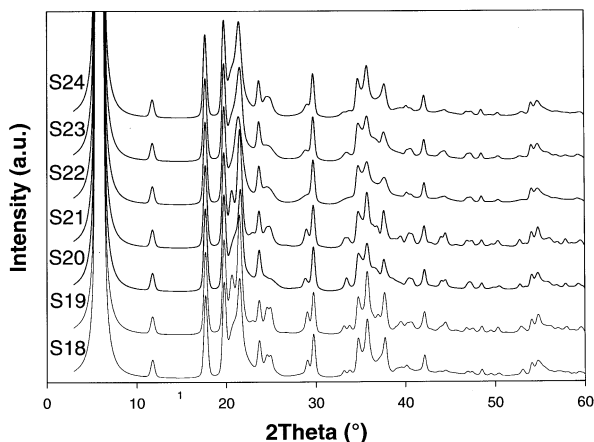**FIGURE 8.** Set of DIFFaX structure simulations of models with rotations between adjacent layers of ±60°, ±120°, and combined ±60° and ± 120°.

with randomly mixed 60° and 120° rotations are S22-S24. It is clear that a model of disorder based only on rotations is unsatisfactory because either the low-intermediate or the high angle regions are poorly modeled. In addition, the peaks at 3.8 and 2.5 Å are always largely overestimated.

DISCUSSION AND FINAL MODEL OF DISORDER

The model of disorder of this Ca-montmorillonite sample may not be directly applied to all montmorillonite samples because, as reported by Weizong et al. (2000), the structure of the clay mineral quasi-crystals depends strongly on the exchangeable cation and H_2O content. Notwithstanding, the working strategy presented here can be successfully utilized for montmorillonite and complex 2:1 clay samples of different nature and this approach can be combined with the method proposed by Reynolds (1993), McCarty and Reynolds (1995), and Drits and McCarty (1996) for a quantitative determination of the content of single units in randomly interstratified mixed-layer structures such as illite-smectite (I/S) to reveal diversity of illite and I/S samples with different conditions of formation and transformation. In addition, it can be employed in the study of mixed-layer phases with integrated TEM and XRD (Guthrie and Reynolds 1998) in an attempt to better account for discrepancies in structure descriptions based only on one technique.

The preliminary structure simulations that consider the variation of all factors which may contribute to the broadening of the diffraction peaks of montmorillonite indicate that a complex model should be used in order to reproduce the observed powder pattern. To this end, we performed simulations with a combination of shifts and rotations, shifts and disordered Al vacancies, and rotations and disordered Al vacancies. In addition, disordering of the Ca atoms and water molecules was also taken into account. Table 5 reports the probability matrices of some selected simulations. In addition to the instrumental contribution, the microstructural broadening was also considered to perfectly reproduce the peak broadening in the observed pattern. Consequently, a finite number of six to seven 15 Å thick layers corresponding to about 10 nm thickness (size of the coherent diffracting domains) was stacked along **c** in agreement with the TEM images and surface area.

Unfortunately, as previously mentioned, our simulations cannot be directly compared with those reported in Drits et al. (1984) because they selected a dehydrated K-saturated montmorillonite system to study the effects of combined disordered models.

Figure 9 shows some selected simulated powder patterns with combinations of shifts and rotations (see the relative probability matrix in Table 5). The Ca atoms are located in the hexagonal cavities. Pattern S25 clearly shows large differences in peak intensities in the 16–25 °2θ region and the presence of the (002) reflection which is not observed in the experimental pattern. The same applies to patterns S26, S27, and S28 although in these cases a better fit of the 16–25 °2θ region was accomplished.

The model which gives the best fit of the observed data (R_p = 0.267) was obtained introducing random shifts along ±**b**/3 and –**a**/3 (see the probability matrix in Table 5) with a total

TABLE 4. The probability of layer existence* and R_p values of structure simulations S18–S24

Simulation	Ideal layer	b/3 shift	−b/3 shift	a/3 shifts	−a/3 shifts	+60° rotation	−60° rotation	+120° rotation	−120° rotation	R_p values†
S18	34	−	−	−	−	33	33	−	−	0.494
S19	20	−	−	−	−	40	40	−	−	0.527
S20	34	−	−	−	−	−	−	33	33	0.484
S21	20	−	−	−	−	−	−	40	40	0.481
S22	20	−	−	−	−	20	20	20	20	0.461
S23	10	−	−	−	−	30	30	15	15	0.471
S24	4					24	24	24	24	0.475

* The probability of existence of the layers is calculated from the probability matrix of DIFFaX. For example, in a model with three layers with a 3 × 3 matrix corresponding to $a_{11} = 20$, $a_{12} = 40$, $a_{13} = 40$, $a_{21} = 40$, $a_{22} = 20$, $a_{23} = 40$, $a_{31} = 40$, $a_{32} = 40$, and $a_{33} = 20$, the probability of existence of each layer is 33%.
† By comparison with the observed file, defined as: $R_p = \{\Sigma |y_i(\text{obs}) - y_i(\text{calc})|\}/\Sigma y_i(\text{obs})$.

TABLE 5. The probability of layer existence* and R_p values of structure simulations S25–S28 and the final obtained model of disorder

Simulation	Ideal layer	Layer b/3	Layer −b/3	Layer a/3	Layer −a/3	Layer 60° rotated	Layer 120° rotated	R_p values†
S25	30	30	30	5	5	−	−	0.368
S26	15	25	25	−	15	20	−	0.365
S27	40	10	10	20	20	−	−	0.351
S28	25	25	25	−	−	−	25	0.357
final	49	23	14	−	23	−	−	0.267
T1‡	−	−	−	−	−	−	−	0.284
T2‡	−	−	−	−	−	−	−	0.286
T3‡	−	−	−	−	−	−	−	0.278

* The probability of existence of the layers is calculated from the probability matrix of DIFFaX. For example, in a model with three layers with a 3 × 3 matrix corresponding to $a_{11} = 20$, $a_{12} = 40$, $a_{13} = 40$, $a_{21} = 40$, $a_{22} = 20$, $a_{23} = 40$, $a_{31} = 40$, $a_{32} = 40$, and $a_{33} = 20$, the probability of existence of each layer is 33%.
† By comparison with the observed file, defined as: $R_p = \{\Sigma |y_i(\text{obs}) - y_i(\text{calc})|\}/\Sigma y_i(\text{obs})$.
‡ Turbostratic models obtained with totally random shifts in the X and Y plane (see text for details).
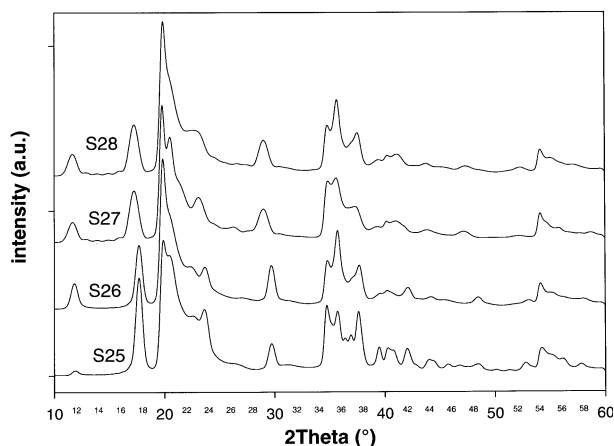

FIGURE 9. Some selected examples of simulated powder patterns with combinations of shifts and rotations (see text and Table 4 for details).

density of defects P_d of 75%.

The idea of a −**a**/3 only plus ±**b**/3 random shifts comes from the observation that the same layer stack is observed in pyrophyllite (Drits et al. 1984). The modulation of the (002) reflection was obtained by disordering the Ca atoms over all possible sites (i.e., both in the hexagonal cavities and under the basal O atom triads) and consequently the distribution of the cations in the octahedral sites is random (either cis and trans sites are occupied). This corresponds with Méring and Glaeser (1954), who suggested that the trans octahedra of the 2:1 layers are occupied by cations to achieve a better local charge balance in the presence of divalent interlayer cations. The chemistry of the Texas montmorillonite is similar to that of sample 1 (Ascan montmorillonite) in Tsipursky and Drits (1984) for which trans octahedral are occupied. These authors also remark that trans

octahedra tend to be occupied in montmorillonites with the charge localized only in octahedra. Figure 10 shows the observed and calculated powder pattern (remember there is no fitting minimization procedure because DIFFaX simply produces a simulated pattern).

It is important at this point to consider turbostratic disorder, the type of disorder that according to Moore and Reynolds (1989) is present in almost all smectite minerals. The series of simulations T1-T3 (Fig. 11) were calculated to reproduce a turbostratic sequence with random shifts in the **a-b** plane and a finite number of 6–7 15 Å thick layers corresponding to about 10 nm thickness (see above). Besides that, T1 was obtained with the Ca atoms and the water molecules in ordered positions in the interlayer region, T2 with the Ca atoms and the water molecules randomly disordered in the **a-b** plane in the interlayer region, and T3 with the Ca atoms and the water molecules randomly disordered in the X, Y, Z planes in the interlayer region (the Z random shifts were restrained so as to have Ca and water molecules at a reasonable bond distance (>2.5 Å) to the basal O atoms. It is clear that especially the simulated powder pattern T3 is very similar to the final model and the observed data. In the light of our results, although a turbostratic model can be applied here, several considerations and issues remain open to debate: (1) In general, it is not possible to state that turbostratic disorder invariably applies to all smectite samples because at least here a better fit to the observed data is obtained using another model which is not fully disordered (random stacking sequence). This model, which is based upon a limited and well defined number of translations, gives the best fit (see the R_p values) because the turbostratic model is not capable of broadening the (002) reflection as well as our model does. (2) It is hard to say where the border between the extensively faulted models such as the one proposed here and the
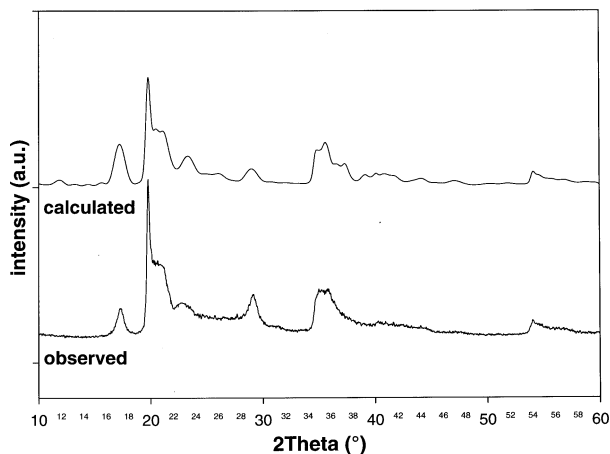
FIGURE 10. The observed pattern of the Ca-montmorillonite and the relative calculated powder pattern using the final model of disorder.
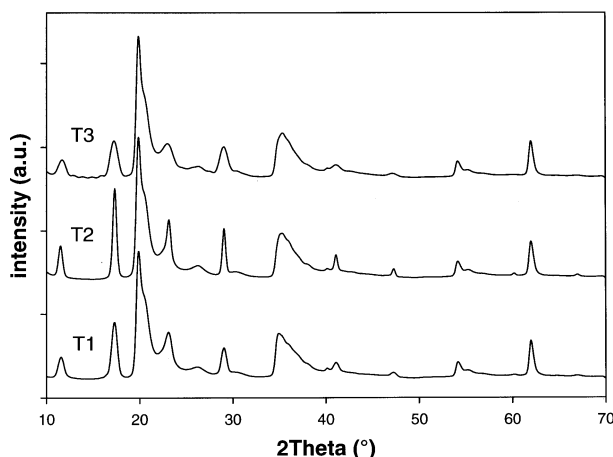

FIGURE 11. Simulations of turbostratic disorder obtained with totally random shifts in the X and Y plane. T1 is obtained with Ca and the water molecules in fixed positions in the interlayer region, T2 with Ca and the water molecules randomly disordered in the X and Y plane in the interlayer region, and T3 with Ca and the water molecules randomly disordered in the X, Y, and Z plane in the interlayer region (see text for further details).

fully disordered (turbostratic) models lies. In fact, our model of disorder has a defect density of 75% (highly faulted) but cannot be considered turbostratic (with predicted defect densities as high as 100%). (3) Is the sample investigated here an exception or is it representative of the real situation? Are other natural samples filling the gap between the random sequences (turbostratic) and the extensively faulted sequences (such as the one proposed here) or can smectite samples be described with both models? (4) Are there other models of disorder? In fact, it turns out that only a model based upon translated sequences (and not rotations) works that excludes the possibility of an equivalence of the rotated and the translated sequences when the interlayer cation is shifted with respect to the center of the "hexagonal" cavity. (5) This result should not be consid-

ered a conclusion but a starting point of discussion and certainly a larger number of samples of different compositions and origins have to be investigated in the future to better assess whether our model is universally applicable.

This disordered model in place of the ideal monoclinic ordered one in the Rietveld QPA analysis is a more reliable input structure model for Ca-montmorillonite yielding more accurate estimates of the weight fractions. As an example, Gualtieri et al. (2000) utilized this model with GSAS (Larson and Von Dreele 1994) by transforming the four-layer recursive model in an approximate deterministic supercell with $c' = 4c$ to fit data of natural clays containing Ca-montmorillonite, which yielded a substantial improvement of the fit and much more accurate weight fractions.

REFERENCES CITED

Allegra, G. (1964) The calculation of the intensity of X-rays diffracted by monodimensionally disordered structures. Acta Crystallographica, 14, 535.
Artioli, G., Bellotto, M., Gualtieri A.F., and Pavese, A. (1995) Nature of disorder in natural kaolinites: a new model based on computer simulation of powder diffraction data and electrostatic energy calculation. Clay and Clay Minerals, 43(4), 438–445.
Bayliss, P. (1989) Unit-cell dimensions of the two-dimensional clay minerals. Powder Diffraction, 4, 19–120.
Bleam, W.F. (1993) Atomic theories of phyllosilicates: quantum chemistry, statistical mechanics, electrostatic theory, and crystal chemistry. Reviews of Geophysics, 31(1), 51–73.
Bray, H.J. and Redfern, S.A.T. (1999) Kinetics of dehydration of Ca-montmorillonite. Physics and Chemistry of Minerals, 26, 591–600.
Brindley, G.W. (1980) Order-disorder in clay mineral structures. In G.W. Brindley and G. Brown, Eds., Crystal Structures of Clay Minerals and their X-ray identification. Mineralogical Society, London, 125–195.
Čapková, P., Driessen, R.A.J., Numan, M., Schenk, H., Weiss, Z., and Klika, Z. (1998) Molecular simulations of montmorillonite intercalated with aluminum complex cations. Part I: intercalation with $[Al_{13}O_4(OH)_{24+x}(H_2O)_{12-x}]^{(7-x)+}$. Clays and Clay Minerals, 46(3), 232–239.
Chang, F.R.C., Skipper, N.T., and Sposito, G. (1997) Monte Carlo and Molecular Dynamics simulations of interfacial structure in lithium-montmorillonite hydrates. Langmuir, 13(7), 2074–2082.
Chatterjee, A., Iwasaki, T., Ebina, T., and Hayashi, H. (1997) Quantum chemical calculation on clay-water interface. Applied Surface Science, 121, 167–170.
Collins, D.R. and Catlow, C.R.A. (1991) Energy-minimized hydrogen-atom positions of kaolinite. Acta Crystallographica, B47, 678–682.
Cowley, J.M. (1976) Diffraction by crystals with planar faults. I. General theory. Acta Crystallographica A, 34, 83–87.
Drits, V.A. and McCarty, D.K. (1996) The nature of diffraction effects from illite and illite-smectite consisting of interstratified trans-vacant and cis-vacant 2:1 layers: A semiquantitative technique for determination of layer-type content. American Mineralogist, 81, 852–863.
Drits, V.A., Plançon, A., Sakharov, B.A., Besson, G., Tsipurski, S.I., and Tchoubar, C. (1984) Diffraction effects calculated for structural models of K-saturated montmorillonite containing different types of defects. Clay Minerals, 19, 541–561.
Gualtieri, A.F. (1999a) Modelling the nature of disorder in talc by simulation of X-ray powder patterns. European Journal of Mineralogy, 11, 521–532.
———(1999b) Accuracy of XRPD QPA using the combined Rietveld-RIR method. Journal of Applied Crystallography, 33, 267–278.
Gualtieri, A.F., Viani, A., Banchio, G. and Artioli, G. (2000) Quantitative phase analysis of natural raw materials containing montmorillonite. Materials Science Forum, 378–381, 702–708.
Guthrie, G.D. and Reynolds, R.C. (1998) A coherent TEM- and XRD-description of mixed-layer illite/smectite. Canadian Mineralogist, 36, 1421–1434.
Güven, N. (1988) Smectites. In S.W. Bailey, Ed., Hydrous Phyllosilicates. Reviews in Mineralogy, Mineralogical Society of America, 19, 497–559.

Hendricks, S. and Teller, E. (1942) X-ray interference in partially ordered layer lattices. Journal of Chemical Physics, 10, 147–167.

Hess, A.C. and Saunders, V.R. (1992) Periodic ab initio Hartree-Fock calculations of the low-symmetry mineral kaolinite. Journal of Physical Chemistry, 96, 4367–4374.

Langford, J.I., Boultif, A., Aufreddic, J.P., and Louër, D. (1993) The use of pattern decomposition to study the combined X-ray diffraction effects of crystallite size and stacking faults in ex-oxalate zinc oxide. Journal of Applied Crystallography, 26, 22–23.

Larson, A.C. and Von Dreele, R.B. (1994) GSAS, General structure analysis system. Los Alamos National Laboratory, document LAUR 86–748.

Louër, D. and Langford, J.I. (1988) Peak shape and resolution in conventional diffractometry with monochromatic X-rays. Journal of Applied Crystallography, 21, 430–437.

McCarty, D.K. and Reynolds, R.C. (1995) Rotationally disordered illite-smectite in Paleozoic K-bentonites. Clays and Clay Minerals, 43, 271–284.

Méring, J. (1975) Smectites in soil components 2. In J.E. Gieseking, Ed., Inorganic components. Springer Verlag, New York, 98–120.

Méring, J. and Glaeser, R. (1954) Sur le role de la valence de cations échangeables dans la montmorillonite. Bulletin Societè Francesè de Mineralogie Cristallographie, 77, 519–522.

Méring, J. and Oberlin, A. (1971) Smectite. In J.A. Card, Ed., The Electron-Optical Investigation of Clays. Mineralogical Society, London, 193–229.

Michalski, E. (1988) The diffraction of X-rays by close-packed polytypic crystals containing single stacking faults. I. General Theory. Acta Crystallographica A44, 640–649.

Michalski, E., Kaczmarek, S., and Demianiuk, M. (1988) The diffraction of X-rays by close-packed polytypic crystals containing single stacking faults. I. Theory for hexagonal and rhomohedral structures. Acta Crystallographica A44, 650–657.

Molloy, M.W. and Kerr, P.F. (1961) Diffraction patterns of A.P.I. reference clay minerals. American Mineralogist, 46, 583–605.

Moore, D.M. and Reynolds, R.C. Jr. (1989) X-Ray diffraction and the identification and analysis of clay minerals. Oxford University Press, Oxford, U.K.

Muller, F., Besson, G., Manceau, A., and Drits, V.A. (1997) Distribution of isomorphous cations within octahedral sheets in montmorillonite from Camp-Bertaux.

Physics and Chemistry of Minerals, 24, 159–166.

Nadeau, P.H. (1985) The physical dimensions of fundamental particles. Clay Minerals, 20, 499–514.

Reynolds, R.C. (1993) Three-dimensional powder X-ray diffraction from disordered illite: simulation and interpretation of the diffraction patterns. In R.C. Reynolds and J. Walker, Eds., Computer Applications to X-ray Diffraction Methods. Clay Minerals Society Workshop Lectures, 5, 44–78.

Sposito, G., Park, S.H., and Sutton, R. (1998) Monte Carlo simulation of the total radial distribution function for interlayer water in sodium and potassium montmorillonites. Clays and Clay Minerals, 47(2), 192–200.

Treacy, M.M.J., Newsam, J.M., and Deem, M.W. (1991) A general recursion method for calculating diffracted intensities from crystals containing planar faults. Proceedings of the Royal Society of London A, 433, 499–520.

Tsipursky, S.I. and Drits, V.A. (1984) The distribution of octahedral cations in the 2:1 layers of dioctahedral smectites studied by oblique-texture electron diffraction. Clay Minerals, 19, 177–193.

Van Berkum, J.G.M., Delhez, R., de Keijser, Th.M., and Mittemeijer, E.J. (1996) Diffraction line broadening due to strain fields in materials; fundamentals aspects and methods of analysis. Acta Crystallographica, A52, 730–747.

Van Olphen, H. and Fripiat, J.J. (1978) Data Handbook for Clay Minerals and other non metallic minerals. Pergamon Press, Oxford.

Warren, B.E. (1959) X-rays studies of deformed metals. Progress in Metal Physics, 8, 147–202.

Weizong X., Johnston, C.T., Parker, P., and Agnew, S.F. (2000) Infrared study of water sorption on Na-, Li-, Ca-, and Mg-exchanged (Swy-1 and Saz-1) montmorillonite. Clays and Clay Minerals, 48, 120–131.

Wilson, A.J.C. (1943) The reflection of X-rays from the 'anti-phase nuclei' of $AuCu_3$. Proceedings of the Royal Society of London A181, 360–368.

Young, R.A. and Wiles, D.B. (1982) Profile shape functions in Rietveld refinements. Journal of Applied Crystallography, 15, 430–438.

Zvyagin, B.B. and Pinsker, Z.G. (1949) Electron diffraction study of the montmorillonite structure. Doklady Academi Nauk SSSR, 68, 30–35.